



HAL
open science

Experimental Investigation of Drying in a Model Porous Medium: Influence of Thermal Gradients

Nicole Vorhauer, Q.T. Tran, Thomas Metzger, Evangelos Tsotsas, Marc Prat

► To cite this version:

Nicole Vorhauer, Q.T. Tran, Thomas Metzger, Evangelos Tsotsas, Marc Prat. Experimental Investigation of Drying in a Model Porous Medium: Influence of Thermal Gradients. *Drying Technology*, 2013, 31 (8), pp.920-929. 10.1080/07373937.2012.724750 . hal-03467246

HAL Id: hal-03467246

<https://hal.science/hal-03467246>

Submitted on 6 Dec 2021

HAL is a multi-disciplinary open access archive for the deposit and dissemination of scientific research documents, whether they are published or not. The documents may come from teaching and research institutions in France or abroad, or from public or private research centers.

L'archive ouverte pluridisciplinaire **HAL**, est destinée au dépôt et à la diffusion de documents scientifiques de niveau recherche, publiés ou non, émanant des établissements d'enseignement et de recherche français ou étrangers, des laboratoires publics ou privés.



Open Archive Toulouse Archive Ouverte (OATAO)

OATAO is an open access repository that collects the work of Toulouse researchers and makes it freely available over the web where possible.

This is an author-deposited version published in: <http://oatao.univ-toulouse.fr/>
Eprints ID: 11024

To link to this article : DOI:10.1080/07373937.2012.724750
URL: <http://dx.doi.org/10.1080/07373937.2012.724750>

To cite this version:

Vorhauer, Nicole and Tran, Q.T. and Metzger, Thomas and Tsotsas, Evangelos and Prat, Marc *Experimental Investigation of Drying in a Model Porous Medium: Influence of Thermal Gradients*. (2013) *Drying Technology* , vol. 31 (n° 8). pp. 920-929. ISSN 0737-3937

Any correspondence concerning this service should be sent to the repository administrator: staff-oatao@listes.diff.inp-toulouse.fr

Experimental Investigation of Drying in a Model Porous Medium: Influence of Thermal Gradients

N. Vorhauer,¹ Q. T. Tran,¹ T. Metzger,¹ E. Tsotsas,¹ and M. Prat²

¹Thermal Process Engineering, Otto von Guericke University, Magdeburg, Germany

²INPT, UPS, IMFT (Institut de Mécanique des Fluides de Toulouse), Université de Toulouse, Toulouse, France, and CNRS, IMFT, Toulouse, France

In this study, isothermal and non-isothermal drying experiments with imposed constant temperature gradients have been conducted in a two-dimensional square pore network of borosilicate glass (SiO₂) with interconnected etched channels. In experiments with temperature decreasing from the open surface of the pore network, a travelling stabilized gas-liquid region could be established, while in isothermal experiments with uniform temperature faster breakthrough and an extended two-phase zone were observed. Both findings are in good agreement with pore network simulations. However, numerical underestimation of drying rates (especially in the second period of drying) indicates that liquid films might play a major role in the experimental pore networks, even in the presence of thermal gradients.

Keywords Etched pore networks; Stabilized drying front; Temperature gradient

INTRODUCTION

The replacement of water by gas through evaporation in the void space of a porous medium during drying can be seen, to a certain extent, as a process of immiscible displacement of a more viscous wetting fluid by a less viscous non-wetting fluid. This explains why concepts developed for the analysis of purely immiscible displacements (drainage) can be useful to analyze drying processes.^[1,2] For this purpose, pore network models,^[3–11] which were originally developed for hydrology and oil-recovery-related applications, can provide a good base to model physical phenomena that occur on the micro scale during drying. Here, capillary liquid transport and vapor diffusion in already dried pores are the main transport mechanisms. However, extended pore network models can also offer a strong tool to model more complex phenomena that proceed during drying, such as crystallization or exposures as shrinkage and cracks that are linked to mechanical effects.^[12,13]

The heat that is demanded for the evaporation of water is commonly supplied by convective dry air, heat conduc-

tion, or radiation. The form of heat input into the porous medium can strongly affect the moisture distribution on the pore level during the drying process^[14–16] and therefore the product quality after drying. Two examples: if drying proceeds with a sharp receding front (i.e., without significant capillary flow), moisture is likely to remain in inner-product pores, demanding either a high effort of energy or time to be completely removed from the product. However, thinking of the impregnation of a solid matrix with a functional solution, capillary flow during the drying step may be undesired because it induces gradients in the applied component. Thus the consideration of the presence of thermal gradients is essential in relation with the applications.

Traditionally, these two key aspects of drying problems, namely the influence of temperature gradients and the evolution of phase distributions, are addressed using mostly phenomenological models (e.g., Whitaker^[17]), and experiments usually involving samples of real porous materials. Although the use of modern techniques such as X-ray computed tomography or NMR techniques can allow the observation of the distribution of phases in a porous medium,^[18] it can be very instructive and much easier to use a simpler approach based on model systems allowing the direct visualization of the phases. These model systems are classically referred to as “micromodel” and are generally two-dimensional networks of interconnected channels.^[19] This type of system has the advantage that the experimental phase distributions observed in the micromodel can be directly compared to the phase distributions obtained by numerical simulations. Also, the network saturation can be derived from the observed phase distributions (by image processing). For these reasons, a micromodel was used for investigations discussed in the present work.

In the same spirit, pore network models can provide a better understanding of the phenomena at the pore level than traditional models.^[3–11] Non-isothermal pore network models have been developed to respect enthalpy differences that can freely evolve inside the pore network due to evaporation (endothermic) and condensation (exothermic), but

Correspondence: Nicole Vorhauer, Thermal Process Engineering, Otto von Guericke University, Universitätsplatz 2, 39106 Magdeburg, Germany; E-mail: nicole.vorhauer@ovgu.de

also to gain a better insight in the dependence of liquid phase distributions on the direction of imposed temperature fields. In particular, the 2D pore network drying simulations reported in Huinink et al.,^[14] Plourde and Prat,^[15] and Surasani et al.^[16] indicate that the invasion by the gas phase resulting from drying can be stabilized if temperatures are higher at the surface than inside the network (temperature field comparable to the one that would develop in a convective drying process). As discussed in more depth in Plourde and Prat,^[15] “stabilized invasion” means that a two-phase zone (i.e., a zone where the gas phase and the liquid phase coexist) of finite width (i.e., the extent of this zone is lower than the medium depth) forms during most of drying. In contrast, if the surface is cold and high temperatures are found at the bottom of the network (temperature field comparable to the one that would develop in contact drying), the invasion is “destabilized” and characterized by the formation of thin gas fingers followed by the development of a second front (i.e., a dry zone) from the network bottom. As discussed in more detail in Plourde and Prat,^[15] these effects are due to the dependence of surface tension on temperature (when the pore size distribution is sufficiently narrow). As pointed out in Huinink et al.,^[14] the dependence of the saturation vapor pressure on temperature can also have a significant impact, at least in the case of the destabilizing gradient.

In the 2D model of Huinink et al.^[14] or Plourde and Prat,^[15] linear temperature profiles between the open and the opposite closed network side are imposed, and constant heat conductivity and stationary heat transport are assumed. In this model, a liquid cluster shrinks if there is a total vapor flux away from this specific cluster (evaporation); in contrast, cluster growth can occur when the net flux is positive (condensation). The condensation effect is, however, only partially taken into account in the model through the refilling of partially empty individual pores (the possible reinvasion of adjacent fully dry pores is not considered). In this respect, it is interesting to obtain information about the possible importance of condensation effects.

In the 2D and 3D non-isothermal drying model of Surasani et al.,^[20] heat and mass transfer equations are coupled and temperature evolves freely (due to heat conduction) depending on evaporation and condensation effects during drying. Drying rate curves (dS/dt) show a significant first drying period (with almost constant drying rate) in the case of the contact heating mode (i.e., cold surface and high temperatures at the sealed bottom of the network) only.^[16] In either case, drying rates drop drastically when surface throats are dried out in the second period of drying. Then, in the third period, drying rates furthermore decrease slightly on a lower level. Although condensation is fully included in the heat transfer equations in the model of Surasani et al.,^[16] it is only partly

respected in the mass transfer: if the net evaporation rate of a cluster is smaller than the net condensation rate, partially filled throats can be refilled. However, refilling of empty throats is not included. Thus, owing to the approximations made in the modelling, comparisons with experiments are highly desirable. This is one of the objectives of the present work, since so far there has been no study aimed at investigating the effect of thermal gradients using micromodel experiments.

It should be mentioned that other publications^[11,21–26] reveal that the decrease of drying rates in the second period can be diminished in the presence of thick liquid films, which remain in the crevices and corners of non-cylindrical pores/throats, while the main liquid front recedes into the network.^[22] They develop due to capillarity effects associated with the presence of corners and other geometrical singularities (roughness) at the pore wall^[21,27,28] and enable hydraulic liquid conduction from the receding drying front towards the evaporation front close to the network surface.^[1] The maximum expansion of the film region is limited by viscous (and gravity) effects, which counteract liquid transport.^[11,26] Although the films can have a quite significant effect on drying rates, previous works indicate that the presence of films does not affect the main features of the phase distributions.^[21,24] In other words, pore network simulations neglecting the films lead to phase distribution during drying in agreement with observations on micromodels (in which films are present). This type of comparison was conducted in the case of isothermal drying.^[4] To the best of our knowledge, comparisons for a non-isothermal case have not been published so far and will be presented in the present article.

In summary, the focus of this paper is the experimental study of the impact of a thermal gradient and the comparison of experimental and computed phase distributions and drying rate curves in the case of uniform temperature ($dT/dz=0$) and for negative temperature gradient ($dT/dz<0$), as mainly observed in convective drying (z is directed from the open edge towards the depth of network, thus a negative thermal gradient means that the temperature decreases as one moves away from the open side of the network). The more complex case of a positive thermal gradient^[14–16] needs further modelling developments because of major condensation effects and will be the subject of a future work.

EXPERIMENTS

Experiments were conducted in a 2D square network of size 50×50 pores with one open side. The micromodel network was produced by photolithography followed by isotropic wet etching of silicon dioxide (SiO_2). Afterwards, the glass structure was sealed by chemical bonding to a silicon (Si) wafer. Due to isotropy of the production process, throats are half cylindrical with two sharp corners



FIG. 1. Cross-section of throats.

(Fig. 1). Width of the pore throats obeys a Gaussian distribution with mean $164\ \mu\text{m}$ and standard deviation $15\ \mu\text{m}$. Throats have uniform length of $1000\ \mu\text{m}$ and uniform depth of $39\ \mu\text{m}$. Saturation of the network with deionized water before drying experiments was conducted in a liquid-filled vacuum chamber; with this method, more than 99.5% of the throats could be saturated with water.

Heat transfer to the network was realized by an aluminium heat conducting plate on which the pore network was mounted (Fig. 2) and which was heated and cooled by two separated, tempered water circuits (one at the open side of the network and one at the opposite side). Temperatures were kept constant during each experiment; the temperature field was recorded once by infrared camera above the network (Camera Image IR 8300, Infratec);

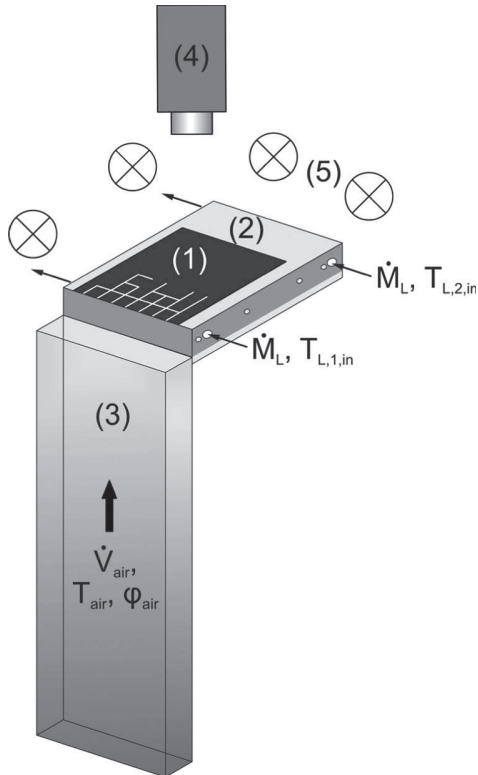


FIG. 2. Sketch of experimental set-up: (1) drying Si-SiO₂ network on heating plate (2) with drill holes for two independent, tempered water circuits with inlet temperatures $T_{L,1,in}$ and $T_{L,2,in}$ and thermo couples; (3) channel for convective dry air perpendicular to open network side; (4) CCD camera or IR camera; (5) LED lights.

during drying, local temperatures were constantly monitored by thermo couples inside the aluminum plate (Fig. 2). The temperature profile recorded with an IR-camera for the experiment with negative temperature gradient is shown in Fig. 3. As depicted in Fig. 3, the temperatures on the hot and cold sides are $T_{\max} = 74^\circ\text{C}$ and $T_{\min} = 53^\circ\text{C}$, respectively. The imposed thermal gradient is therefore $dT/dz \approx -0.43\ \text{K mm}^{-1}$. As can be seen, the temperature gradient is spatially not perfectly constant. Except on the edges, the isothermal lines are, however, parallel to the open edge of network.

Drying of the network was realized with a convective flow of dry air (with an absolute humidity below $0.001\ \text{kg H}_2\text{O/kg dry air}$) at room temperature ($\bar{T}_{air} = 24.3^\circ\text{C}$ in the isothermal experiment and $T_{air} = 25.2^\circ\text{C}$ in the non-isothermal experiment) perpendicular to the open side of the network ($\dot{V}_{air} = 201\ \text{min}^{-1}$) (Fig. 2). As the top cover of the network (SiO₂) is transparent, drying (i.e., stepwise emptying of throats) could be constantly monitored with a CCD camera. Illumination of the network was realized by power LED lights on top and on the four sides of the network (Fig. 2). A good light setting was the most important requirement for the experimental set-up in order to reduce misinterpretation of the state of individual throats (full or empty).

From the sequence of images taken during experiments, drying curves (as shown later in Fig. 10) are derived by image processing (binarization and segmentation of images). For this, the original RGB color images are converted into binary images, in which pixels, representing the gas phase, have the numerical value 1 and pixels, representing the liquid phase (and the solid), have the value 0. Throat saturations S_{ij} are derived from the sum of white pixels inside a throat (i.e., from the number of total pixels inside a throat reduced by the sum of white pixels). Then,

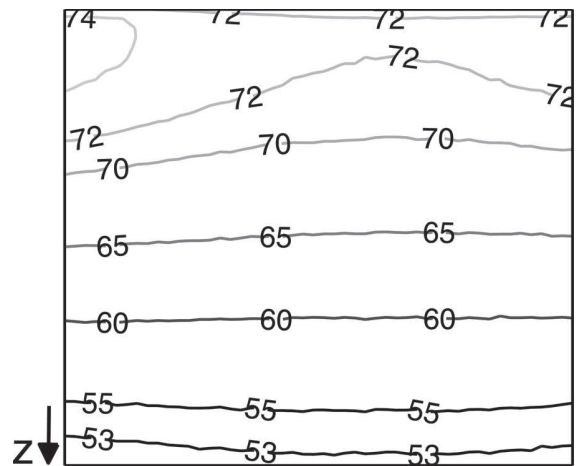


FIG. 3. Temperature field (in $^\circ\text{C}$) as monitored by an infrared camera in the experiment with negative thermal gradient.

the drying curve $S(t)$ is obtained from overall network saturation S evaluated at different points in time

$$S = \frac{\sum_{ij=1}^{N_t} (S_{ij} \cdot V_{ij}) + \sum_{i=1}^{N_p} (S_i \cdot V_i)}{\sum_{ij=1}^{N_t} V_{ij} + \sum_{i=1}^{N_p} V_i} \quad (1)$$

with throat/pore saturation S_{ij} and S_i and throat/pore volume V_{ij} and V_i , respectively. The experimental drying rate curves shown later in Fig. 11 are then derived from the slope of the drying curve (dS/dt) by application of a moving average filter.^[26]

PORE NETWORK MODEL

The pore network model is based on models reported in Huinink et al.^[14] and Plourde and Prat.^[15] Details and specifications are described in the following. In the pore network model, the void space of porous media is represented by a two-dimensional regular square lattice of discrete pores (i, j, k) and throats (ij, jk) with a Gaussian distribution of throat size (as sketched in Fig. 4). For simplicity, the cross section of throats is assumed to be rectangular, thus close to the experimental shape (Fig. 1). Computational nodes are also located in the free gas above the pore network so as to include the external mass boundary layer in the computation. This is useful for a better representation of mass transfer at the open surface of the network.^[16,29]

In drying simulations, the total void space is initially saturated with water, then evaporation starts from the open side of the network (all other sides of the network are impermeable for mass transfer). The network configuration is in a

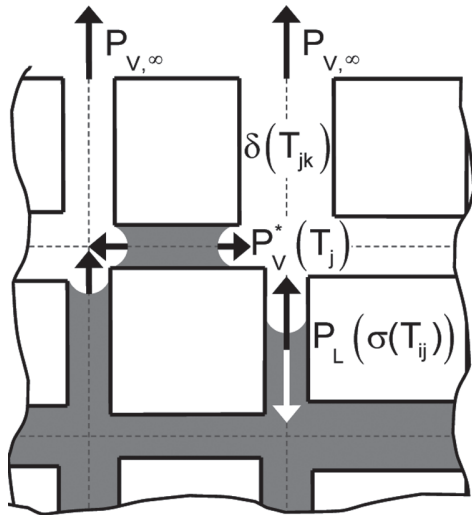


FIG. 4. Schematic representation of the 2D pore network model and relevant transport mechanisms; liquid phase in grey and gas phase in white.

horizontal position (as in experiments) so that gravity effects are negligible. For non-isothermal drying simulation, the steady-state temperature field from experimental measurements (Fig. 3) is imposed on the pore network.

In the discrete pore network model, mass balances of individual gas and liquid throats (set of linear equations) are solved stepwise.^[30] Because of moderate evaporation rates and relatively large throats, viscosity effects in the liquid phase are disregarded in the model and liquid throats empty in the order of decreasing liquid pressure during drying.^[3] Liquid transport in full ($S_{ij} = 1$) and partially saturated ($0 < S_{ij} < 1$) throats ij (Fig. 4) is a result of the so-called “capillary pumping effect,” which is due to liquid pressure gradients usually existing between small throats (where the pressure is lower) and large throats (where the pressure is higher), as described by the phenomenological equation of Laplace,

$$P_{L,ij} = P - P_{C,ij} = P - \frac{2\sigma(T_{ij})}{\bar{r}_{ij}} \quad (2)$$

with total pressure P of gas phase, capillary pressure $P_{C,ij}$ of throat ij , temperature-dependent surface tension σ , and mean radius of curvature \bar{r}_{ij} ,

$$\bar{r}_{ij} = \frac{2 \cdot r_{ij} \cdot (L_d/2)}{r_{ij} + (L_d/2)} \quad (3)$$

with throat depth L_d . As reported in Plourde and Prat,^[15] the situation can be different in the presence of a thermal gradient owing to the variation of surface tension σ of water with temperature T ,^[16]

$$\sigma(\text{N} \cdot \text{m}^{-1}) = -1.704 \cdot 10^{-4} \cdot T(^{\circ}\text{C}) + 7.636 \cdot 10^{-2}. \quad (4)$$

Since the surface tension of water is a decreasing function of temperature, the effect of temperature is to favour the capillary pumping from the hot throats (where the liquid pressure is higher for a given throat size according to Eq. (2)) towards the cold throats. Because both the throat size distribution and the temperature gradient affect the invasion, various situations are possible depending on which effect is dominant (see Plourde and Prat^[15] for more details).

For the system considered in the present article, Fig. 5 shows that the dependency of liquid pressure P_L on temperature is not negligible compared to the dependence upon the throat size r , especially if one remembers that the range of throat sizes involved in the invasion of the main cluster (i.e., the largest cluster in the system) is narrower than the full range (the “active” throat size range is actually roughly $[\bar{r}, r_{\max}]$, where \bar{r} denotes the mean throat size and r_{\max} the largest throat size). Figure 5 illustrates that a throat of size \bar{r} at temperature

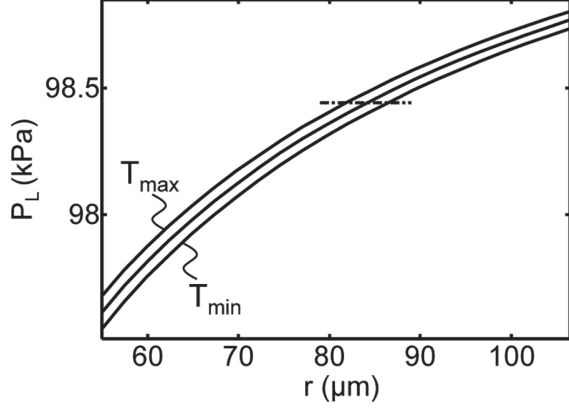


FIG. 5. Liquid pressure dependency P_L on throat size for throat temperatures T_{\min} , \bar{T} , and T_{\max} .

T_{\max} can produce the same liquid pressure as a throat larger than \bar{r} but at the lower temperature T_{\min} (dotted line in Fig. 5).

At the gas liquid interface, local thermodynamic evaporation equilibrium with saturation vapor pressure P_V^* at pore temperature T_j is assumed (Fig. 4). The dependency of water saturation vapor pressure on temperature is an exponential function, which can be calculated with an empirical Antoine equation. Vapor transfer in the gas phase is based on vapor pressure gradients between the phase boundary (P_V^*) and the surrounding gas phase ($P_{V,\infty} = 0$), which in the model is specified in the last pore row of the boundary layer. The mass flow rate of vapor $\dot{M}_{V,ij}$ through a throat ij can be described with a linear diffusion approach, which is combined with Stefan correction:

$$\dot{M}_{V,ij} = A_{ij} \frac{\delta(T_{ij})}{L_{ij}} \frac{P \tilde{M}_V}{R T_{ij}} \ln \left(\frac{P - P_{V,i}}{P - P_{V,j}} \right) \quad (5)$$

where A_{ij} is the cross-sectional area of the throat ij , δ denotes the vapor diffusion coefficient, \tilde{M}_V the molar mass of vapor, L_{ij} the throat length, R the ideal gas constant and $P_{V,i}$ the vapor pressure in adjacent pore i . Vapor diffusion benefits from high temperatures as the vapor diffusivity δ of water is temperature-dependent as follows:^[31]

$$\delta (m^2 \cdot s^{-1}) = \frac{22.6 \cdot 10^{-6}}{P(\text{bar})} \cdot \left(\frac{T_{ij}(K)}{273} \right)^{1.81} \quad (6)$$

In non-isothermal systems, condensation of vapor occurs if the local partial vapor pressure is higher than the saturation vapor pressure.^[14–16] In simulations, condensation at menisci throats is respected in those cases in which incoming vapor fluxes of pore j are higher than the outgoing vapor fluxes (Fig. 6)^[14]

$$\dot{M}_{V,ij} + \dot{M}_{V,kj} > \dot{M}_{V,j\infty} \quad (7)$$

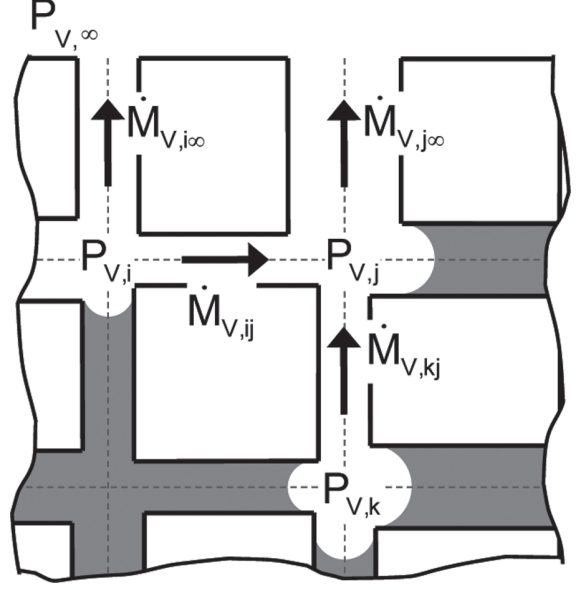


FIG. 6. Condensation at liquid menisci.

Condensation at cluster menisci leads to a decrease of the overall cluster evaporation rate,

$$\dot{M}_{V,Cl} = \sum_{i=1}^{i=NMT} \dot{M}_{V,i}^{ev} - \sum_{i=1}^{i=NMT} \dot{M}_{V,i}^{con} \quad (8)$$

However, the overall cluster evaporation rate can not become negative (as refilling of throats and pores is not considered), so that in this case the theoretically condensing liquid is neglected; this can be interpreted as a numerical sink. In general, condensation effects lead to a reduction of the overall drying rate. Especially in the heating mode with cold open network side and hot network bottom (positive temperature gradient), where vapor is diffusing in the direction of decreasing temperatures, condensation plays a major role. Theoretical prediction of drying in this case requires the inclusion of imbibition mechanisms in the present model; this will be the focus of a future work.

ISOTHERMAL VS NON-ISOTHERMAL DRYING

Drying experiments in pore networks are relatively long duration experiments which can take up to several days or even weeks (especially isothermal experiments at room temperature). Due to this, repetition of experiments (of high quality) in a high quantity is not always possible. Hence, here only the results of one experiment for each parameter setting shall be discussed. The experimental phase distributions for a constant temperature of $T = 63^\circ\text{C}$ are shown together with the simulated phase distributions in Figs. 7a–h and the phase patterns of the non-isothermal case with $dT/dz \approx -0.43 \text{ K mm}^{-1}$ are shown in Figs. 8a–h.

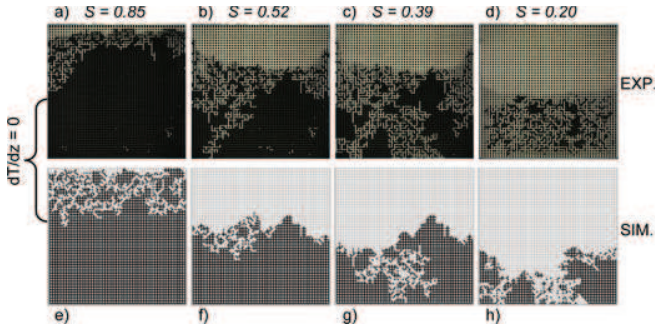


FIG. 7. Isothermal experimental (up row) and theoretical (down row) phase distributions at different network saturations S : a) when liquid phase detaches from the open network surface (on top) in experiment at $S=0.85$, in the theoretical phase distribution individual surface throats are still wet (detachment at $S=0.82$); b) phase patterns for $S=0.52$ (breakthrough of gas phase in experiment); c) $S=0.39$ (theoretical breakthrough); and d) $S=0.2$. Liquid throats are in black and gas throats in white. In the experimental image sequence, liquid films can be found in throats with an intermediate grey value (Labels e) to h) are referred to in the main text.) (color figure available online).

If no temperature gradient is applied the throat potential (to empty) is depending on the throat size only (large throats are preferentially invaded), and individual gas branches can easily penetrate the network. As can be seen from the experimentally obtained phase distributions (Figs. 7a–d), the result is a classical invasion percolation pattern with progressive evaporation of isolated liquid clusters.^[3] In this case, the phase distribution is characterized by two main zones: a dry zone adjacent to the open edge (on top) and a two-phase zone where liquid and gas throats coexist. As depicted in Fig. 7b–d, the dry zone expands during drying whereas the two-phase zone progressively shrinks.

Figures 8a–h show the phase patterns in the presence of a negative thermal gradient between the open network side and the sealed bottom. As can be seen, the application of

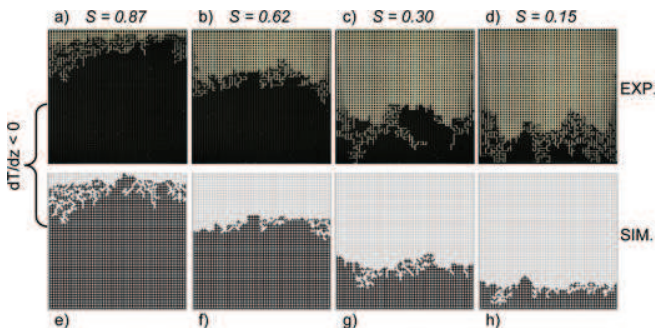


FIG. 8. Phase distributions as obtained by experiments and simulations with $dT/dz < 0$: a) phase distributions for $S=0.87$ (experimental detachment of the liquid phase); b) $S=0.62$; c) $S=0.30$ (experimental breakthrough); and d) $S=0.15$ (theoretical breakthrough). (Labels e) to h) are referred to in the main text.) (color figure available online).

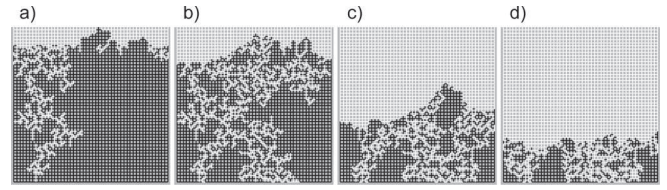


FIG. 9. Simulated drying patterns for $dT/dz < 0$, assuming the surface tension independent of temperature: a) breakthrough occurs at $S=0.795$; phase patterns for b) $S=0.62$; c) $S=0.3$; and d) $S=0.15$.

a temperature gradient markedly affects the phase distribution during drying. In contrast with the isothermal case, drying in this case is characterized by the formation of three main zones (instead of two): the expanding dry zone adjacent to the open edge, a shrinking liquid-saturated zone adjacent to the sealed bottom side of network and, in between, a travelling two-phase zone. The two-phase zone is therefore of finite size; its size is always significantly narrower than the network depth. This type of drying pattern is referred to as a stabilized invasion pattern (see Prat and Bouleux^[32] for more details). As discussed in Plourde and Prat^[15] and Huinink et al.,^[14] two main effects can be invoked to explain the change in the invasion pattern due to the thermal gradient. The first one is due to the dependence of surface tension on temperature.^[15] As mentioned before, the surface tension is decreasing with temperature (Eq. (4)). As a result, it is comparatively easier to invade the throats of higher temperature. This changes the order in which the throats are successively invaded compared to the isothermal case. As reported in Plourde and Prat,^[15] this effect is sufficient to obtain a stabilized pattern if the (negative) temperature gradient is high enough to overcome in part the effect of geometrical disorder (the throat size spatial variations). The second effect is due to the dependence of saturation vapor pressure on temperature. Since the saturation vapor pressure increases with temperature, the temperature gradient induces a negative saturation vapor pressure gradient across the two-phase zone. As a result, a mass flux in the gas phase takes place from the warmer region of two-phase zones towards colder regions. This enables the liquid supply of clusters located deeper in the network by condensation of the vapor produced in the warmer regions located closer to the dry zone. The simulations reported in Huinink et al.^[14] suggest, however, that this latter effect is not sufficient to significantly affect the pattern. Thus the surface tension effect should explain the change in the pattern when the thermal gradient is imposed. This will be confirmed by the numerical simulations discussed in the next section.

EXPERIMENTS VS. PORE-NETWORK SIMULATIONS

Comparable phase distributions are obtained with the pore network simulations, as can be seen from Figs. 7e–h

and Figs. 8e–h, respectively. Simulations have been conducted with the same pore network as in the experiment; for the theoretical investigation of non-isothermal drying the temperature field as measured during the experiment (Fig. 3) was applied. Theoretical boundary layer thickness was adapted so as to describe the initial experimental drying rates. In the isothermal pore network, a boundary layer thickness of $s_{BL} = 800 \mu\text{m}$ was used; in the non-isothermal pore network the estimated boundary layer thickness is $s_{BL} = 250 \mu\text{m}$. For simulations, temperature of the convective dry air was implemented as measured during experiments and zero humidity ($P_{v,\infty} = 0$) was assumed.

Isothermal Case

As can be taken from the phase distributions in Fig. 7, individual gas branches are penetrating the liquid phase at the beginning of drying, in both experiment and simulation, if no temperature gradient is applied. Owing to the formation of isolated clusters (Figs. 7a, 7e) which tend to evaporate more rapidly since they are not fed by the liquid located deeper in the network, the liquid phase detaches from the open network side (i.e., when the first vertical and horizontal network slices are empty) at a saturation of $S = 0.85$ in the experiment (Fig. 7a) and $S = 0.82$ in the simulation. Evaporation occurs at the least advanced points where the gas throats are at saturation vapor pressure. The evaporation front thus corresponds to the interface between the two-phase zone and the dry zone (if one disregards the film effects discussed in the next section); it recedes into the network with decreasing network saturation. However, one can also observe that the position of the least advanced point of the front remains constant over a significant time period (Figs. 7b–c) as long as liquid pumping from the network bottom to the least advanced point of the front is sustained within the main connected cluster; under isothermal conditions the vapor pressure gradient between most and least advanced point of the front goes to zero because vapor pressure in the gas throats within the two-phase zone is essentially equal to the saturation vapor pressure because of a confinement effect. Thus the evaporation rate is essentially zero inside the two-phase zone (this is referred to as a screening effect, since menisci within the two-phase zone do not participate in evaporation). When the main cluster splits up into smaller separated clusters, liquid pumping is interrupted and the liquid level continues receding into the network ($S = 0.2$, Fig. 7d). It should be mentioned that in the experiment the liquid phase detaches from the three sealed sides of the network (Fig. 7d) and at the end of drying the last liquid throat is not connected to the bottom of the network (as found in the simulation).

Breakthrough occurs at a significantly lower network saturation in the simulation ($S = 0.39$) (Fig. 7g) than in the experiment ($S = 0.52$) (Fig. 7b), although the least advanced point of the main liquid cluster is almost at the

same position in both cases (Figs. 7b, 7g). An explanation might be the trapping of single liquid clusters in the simulation: when single clusters are separated from the main cluster at the evaporation front, capillary liquid pumping from the main cluster is interrupted. Due to the screening effect, separated clusters must dry out from the open network side before gas invasion can further proceed in the depth of the network. This can lead to an intermittent stabilization of the front (Fig. 7f). The situation seems to be different in the experiment: here the observed number of individual clusters is higher for a given overall network saturation as they can survive for a longer time period (Figs. 7b–c). This could be an indication for liquid films that would enable an interconnection of single clusters and their liquid supply from deeper network regions.

Negative Temperature Gradient

Detachment of liquid phase from the open network side is, in both cases, found at higher overall network saturations than in the isothermal case: $S = 0.87$ in experiment and $S = 0.86$ in simulation (Figs. 8a, 8e). Furthermore, breakthrough occurs significantly earlier in the experiment ($S = 0.30$) (Fig. 8c) than in the simulation ($S = 0.15$) (Fig. 8h).

As can be seen from Fig. 8, the stabilizing effect of the temperature gradient is well reproduced by the pore network simulation. As in the experiment, a well-defined travelling two-phase zone is obtained between the dry zone and a still fully saturated liquid zone. The numerical simulation can help us to understand the mechanisms leading to the formation of a stabilized pattern when $dT/dz < 0$. Figure 9 shows the drying patterns for the case of $dT/dz < 0$ when the dependency of temperature on surface tension is neglected. Except for the surface tension, which is assumed to be independent of temperature ($\sigma = 72.74 \cdot 10^{-3} \text{N m}^{-1}$), all other parameters have the same values as the ones leading to the patterns shown in Fig. 8. The patterns depicted in Fig. 9 are clearly very close to the ones corresponding to the isothermal case in Fig. 7. This demonstrates that the leading effect, which is stabilizing the pattern, is the gradient in the surface tension imposed by the temperature gradient as discussed in Plourde and Prat.^[15] The simulations also indicate that condensation effects can be neglected in the case of $dT/dz < 0$. The condensation effect discussed in the previous section was indeed obtained numerically but was not sufficient to compensate or overcome the evaporation taking place at other menisci along the boundaries of liquid clusters. This is in agreement with the experiment where the significant growth of clusters due to condensation was not observed.

DRYING RATES

The simulated drying curves and drying rate curves are shown together with the experimental curves in Figs. 10 and 11, respectively.

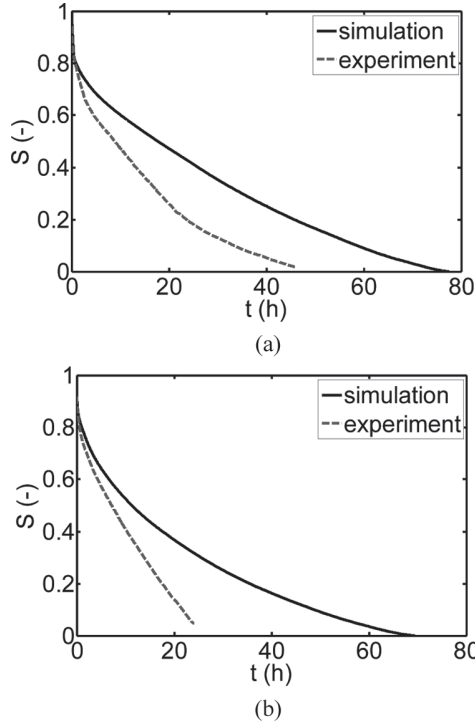


FIG. 10. Experimental and theoretical drying curves for a) $dT/dz=0$ and b) $dT/dz < 0$.

The drying rate curves are characterized by the absence of a constant rate period (CRP),^[33–34] in which initial drying rates are constant. The absence of CRP is classical for 2D systems in the first drying period and is due to the percolation properties of the two-phase zone in 2D, which are markedly different from the 3D case (Prat et al.^[35] and references therein). The drying rate curve is essentially characterized by a short falling rate period (FRP) in which the drying rate drastically drops, followed by a long receding front period (RFP), which is characterized by the evaporation front receding into the network and a slight decrease of drying rates on a low level.^[35]

The most striking result in Figs. 10 and 11 is that the drying rates are underestimated by the numerical simulations during the RFP. This holds for both the isothermal case and the negative temperature gradient. The simulated total drying time is almost twice as large as the experimental time in the isothermal case and about three times as large in the presence of the negative temperature gradient. Since the simulated drying rates are lower during the RFP, where the drying rate is controlled by the internal transport phenomena (the external mass transfer resistance is negligible during the RFP), this indicates that a significant effect is missing in the pore network model as regards the computation of internal evaporation flux. In other words, the pore network model is in good agreement with experiments in terms of the phase distributions (Figs. 7 and 8), but there

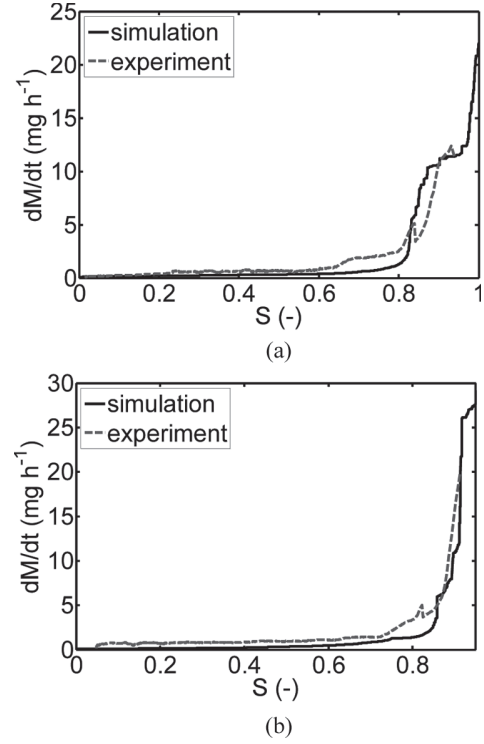


FIG. 11. Experimental and theoretical drying rate curves for a) $dT/dz=0$ and b) $dT/dz < 0$. For illustration purposes, saturations of $S > 0.95$ are not shown for the non-isothermal case; the initial drying rate ($S = 1$) is $dM/dt = 107 \text{ mg h}^{-1}$.

is a noticeable difference in terms of the drying rates. According to previous works (e.g., Laurindo and Prat^[21] and Prat^[11,24] and references therein), the most likely explanation for this might be found in the presence of liquid films which can be observed in the corners of the non-cylindrical throats during experiments. In the experimental images in Figs. 7 and 8, liquid films appear in gas-invaded throats with a different grey value compared to totally dried throats (which are white). This is particularly visible in Figs. 7b–d. As demonstrated from a simple experiment of drying of a capillary tube of square cross-section, liquid films contribute to liquid conduction as they act as a secondary capillary system (with small radii compared to the width of the throat).^[26] In the presence of films, individual liquid clusters are also not separated from each other but connected by corner film flow. For this reason, individual liquid clusters can be supplied with liquid and survive for a longer period in experiments (Figs. 7b–c), contrary to simulations where separated single clusters dry out (Figs. 7f–g). Furthermore, the films enable liquid transport up to the evaporation front: the net effect is a mean position of the evaporation front closer to the network open side than predicted in the absence of films. (Of course the width of the film region is limited due to the small radii of corner films and the vis-

cosity of liquid, hence the film region must also recede into the network during drying). The effective dry zone is therefore narrower owing to film action, which leads to higher drying rates than predicted with the pore-network model (which does not take into account the film effect); this is, for example, discussed in Prat.^[11] It is therefore desirable to include the film effects in the model for a better assessment of drying rates. This has been done in previous works (e.g., Yiotis et al.,^[22] Prat,^[24] and Segura^[25]), but not in the presence of a thermal gradient.

CONCLUSIONS AND OUTLOOK

Isothermal ($dT/dz = 0$) and non-isothermal ($dT/dz < 0$) drying experiments have been conducted in a Si-SiO₂ pore network with 50×50 pores. In non-isothermal drying experiments, a constant temperature field with high temperatures at the open side of the 2D pore network (as expected in convective drying) was imposed by means of a heat conducting plate and monitored with an infrared camera. The experiment nicely confirms previous numerical predictions in terms of the stabilizing effect of a negative temperature gradient. The new pore network simulations presented in the article confirm that the stabilizing effect is due to the gradient in the surface tension induced by the thermal gradient. The experiment and the simulations indicate that the condensation effect associated with the variation of saturation vapor pressure across the two-phase zone is negligible.

In both the isothermal and non-isothermal cases, experimental drying rates were significantly higher than predicted by pore network simulations. Based on previous works, the most likely explanation lies in the effect of thick liquid films. Thick liquid films are visible in the experiment along the edges and corners of the non-cylindrical throats of the Si-SiO₂ network in regions where the throats are invaded by the gas phase. Interestingly, the films are visible not only in the isothermal case but also in the non-isothermal case. The comparisons between experiments and simulations presented in this article confirm that the presence of liquid films has a limited influence on the main features of phase patterns but that drying rates can be significantly higher due to the efficient transport mechanism of liquid by films in throats mainly occupied by the gas phase. Further investigation should therefore address experimental and theoretical evaluation of the contribution of thick liquid films to the overall drying behavior in our system, especially in the presence of a thermal gradient.

NOMENCLATURE

A	Cross-sectional area (m ²)
L	Throat length (m)
L _d	Throat depth (m)
M	Mass (kg)

\dot{M}	Mass flow rate (kg s ⁻¹)
\bar{M}	Molar mass (kg kmol ⁻¹)
NMT	Number of meniscus throats
N _p	Number of pores
N _t	Number of throats
P	Pressure (Pa)
r	Throat radius (m)
\bar{r}	Mean throat radius (m)
\bar{R}	Ideal gas constant (kJ kmol ⁻¹ K ⁻¹)
s _B L	Boundary layer thickness (m)
S	Saturation
t	Time (s)
T	Temperature (°C)
\bar{T}	Mean temperature (°C)
\dot{V}	Flow rate (m ³ h ⁻¹)
z	Distance to network surface (m)
δ	Gas diffusivity (m ² s ⁻¹)
ΔT	Temperature gradient (K)
σ	Surface tension (N m ⁻¹)
φ	Relative humidity (-)

Subscripts and Superscripts

0	Reference
1,2	(Temperature) level
air	Air
C	Capillary
Cl	Cluster
con	Condensation
ev	Evaporation
i, j, k	Pore indices
ij, jk	Throat indices
in	Inlet
L	Liquid
max	Maximum value
min	Minimum value
V	Vapor
*	Equilibrium
∞	Bulk air

ACKNOWLEDGMENTS

The first author wants to thank the Institute of Micro and Sensor Technique, Otto von Guericke University, for the production of Si-SiO₂ pore networks of very high precision. Part of the experimental equipment was financed by the Graduate School Micro-Macro (DFG GRK1554). The second author was financed by Stiftung Industrieforschung. The cooperation between the institutes was financed by Deutsch-Französische-Hochschule (DFH-UFA).

REFERENCES

1. Shaw, T.M. Drying as an immiscible displacement process with fluid counterflow. *Physical Review Letters* **1987**, *59*, 1671–1674.

2. Yiotis, A.G.; Tsimpanogiannis, I.N.; Stubos, A.K. Experimental study of drying/evaporation in an effective 2-D porous medium. *Proceedings of NSTI-Nanotech* **2010**, *2*.
3. Prat, M. Percolation model of drying under isothermal conditions in porous media. *International Journal of Multiphase Flow* **1993**, *19*(4), 691–704.
4. Laurindo, J.B.; Prat, M. Numerical and experimental network study of evaporation in capillary porous media: Phase distributions. *Chemical Engineering Science* **1996**, *51*(23), 5171–5185.
5. Tsimpanogiannis, I.N.; Yortsos, Y.C.; Poulou, S.; Kanellopoulos, N.; Stubos, A.K. Scaling theory of drying in porous media. *Physical Review E* **1999**, *59*(4), 4353–4365.
6. Le Bray, Y.; Prat, M. Three-dimensional pore network simulation of drying in capillary porous media. *International Journal of Heat and Mass Transfer* **1999**, *42*, 4207–4224.
7. Yiotis, A.G.; Stubos, A.K.; Boudouvis, A.G.; Yortsos, Y.C. A 2-D pore-network model of the drying of single-component liquids in porous media. *Advances in Water Resources* **2001**, *24*, 439–460.
8. Prat, M. Recent advances in pore-scale models for drying of porous media. *Chemical Engineering Journal* **2002**, *86*(1–2), 153–164.
9. Segura, L.A.; Toledo, P.G. Pore-level modeling of isothermal drying of pore networks accounting for evaporation, viscous flow, and shrinking. *Drying Technology* **2005**, *23*, 2007–2019.
10. Metzger, T.; Irawan, A.; Tsotsas, E. Isothermal drying of pore networks: Influence of friction for different pore structures. *Drying Technology* **2007**, *25*, 49–57.
11. Prat, M. Pore network models of drying, contact angle and film flows. *Chemical Engineering and Technology* **2011**, *34*(7), 1029–1038.
12. Veran-Tissoires, S.; Marcoux, M.; Prat, M. Discrete salt crystallization at the surface of a porous medium. *Physical Review Letters* **2012**, *108*, 054502.
13. Kharaghani, A.; Metzger, T.; Tsotsas, E. A proposal for discrete modeling of mechanical effects during drying, combining pore networks with DEM. *AIChE Journal* **2011**, *57*, 4.
14. Huinink, H.P.; Pel, L.; Michels, M.A.J.; Prat, M. Drying processes in the presence of temperature gradients: Pore-scale modelling. *European Physical Journal E* **2002**, *9*, 487–498.
15. Plourde, F.; Prat, M. Pore network simulations of drying of capillary porous media: Influence of thermal gradients. *International Journal of Heat and Mass Transfer* **2003**, *46*, 1293–1307.
16. Surasani, V.K.; Metzger, T.; Tsotsas, E. Influence of heating mode on drying behavior of capillary porous media: Pore scale modelling. *Chemical Engineering Science* **2008**, *63*, 5218–5228.
17. Whitaker, S. Simultaneous heat, mass and momentum transfer in porous media: A theory of drying. *Advances in Heat Transfer*; Academic Press: New York, 1977; 13.
18. Van der Heijden, G.H.A.; Huinink, H.P.; Pel, L.; Kopinga, K. Non-isothermal drying of fired-clay brick, an NMR study. *Chemical Engineering Science* **2009**, *64*, 3010–3018.
19. Lenormand, R.; Touboul, E.; Zarcone, C. Numerical models and experiments on immiscible displacements in porous media. *Journal of Fluid Mechanics* **1988**, *189*, 165–187.
20. Surasani, V.K.; Metzger, T.; Tsotsas, E. Consideration of heat transfer in pore network modelling of convective drying. *International Journal of Heat and Mass Transfer* **2008**, *51*, 2506–2518.
21. Laurindo, J.B.; Prat, M. Numerical and experimental network study of evaporation in capillary porous media: Drying rates. *Chemical Engineering Science* **1998**, *53*(12), 2257–2269.
22. Yiotis, A.G.; Boudouvis, A.G.; Stubos, A.K.; Tsimpanogiannis, I.N.; Yortsos, Y.C. Effect of liquid films on the drying of porous media. *AIChE Journal* **2004**, *50*(11), 2721–2731.
23. Yiotis, A.G.; Tsimpanogiannis, I.N.; Stubos, A.K.; Yortsos, Y.C. Coupling between external and internal mass transfer during drying of a porous medium. *Water Resources Research* **2007**, *43*.
24. Prat, M. On the influence of pore shape, contact angle and film flows on drying of capillary porous media. *International Journal of Heat and Mass Transfer* **2007**, *50*, 1455–1468.
25. Segura, L.A. Modeling at pore-scale isothermal drying of porous materials: Liquid and vapor diffusivity. *Drying Technology* **2007**, *25*, 1677–1686.
26. Chauvet, F.; Duru, P.; Geoffroy, S.; Prat, M. Three periods of drying of a single square capillary tube. *Physical Review Letters* **2009**, 103.
27. Lenormand, R.; Zarcone, C. Role of roughness and edges during imbibition in square capillaries. *The Society of Petroleum Engineers Journal* **1984**, 13264–MS.
28. Chauvet, F.; Duru, P.; Prat, M. Evaporation in square capillary tubes: Optical measurement of the corner films thickness. In *7th World Conference on Experimental Heat Transfer, Fluid Mechanics and Thermodynamics*, Krakow, Poland, 2009.
29. Irawan, A.; Metzger, T.; Tsotsas, E. Pore network modelling of drying: Combination with a boundary layer model to capture the first drying period. In *Proceedings of 7th World Congress of Chemical Engineering*, Glasgow, Scotland, 10–14 July 2005.
30. Metzger, T.; Tsotsas, E.; Prat, M. Pore-network models: A powerful tool to study drying at the pore level and understand the influence of structure on drying kinetics. In *Modern Drying Technology, Vol. 1: Computational Tools at Different Scales*; Tsotsas, E., Mujumdar, A.S., Eds.; Wiley-VCH: Weinheim, 2007; 57–102.
31. Schirmer, R. Die Diffusionszahl von Wasserdampf-Luftgemischen und die Verdampfungsgeschwindigkeit. *VDI Beiheft Verfahrenstechnik* **1938**, 170–177.
32. Prat, M.; Bouleux, F. Drying of capillary porous media with stabilized front in two-dimensions. *Physical Review E* **1999**, *60*, 5647–5656.
33. Van Brakel, J. Mass transfer in convective drying. In *Advances in Drying I*; Mujumdar, A.S., Ed.; Hemisphere: New York, 1980; 217–267.
34. Krischer, O.; Kast, W. *Trocknungstechnik Erster Band: Die wissenschaftlichen Grundlagen der Trocknungstechnik*, 3; Auflage, Springer-Verlag: Heidelberg, 1992.
35. Prat, M.; Veran-Tissoires, S.; Vorhauer, N.; Metzger, T.; Tsotsas, E. Fractal phase distribution and drying: impact on two-phase zone scaling and drying time scale dependence. *Drying Technology* **2012**, *30*, 1129–1135.